Numer. Math. Theor. Meth. Appl.
doi: 10.4208/nmtma.2015.m1403

Vol. **8**, No. 4, pp. 530-548
November 2015

# A Lions Domain Decomposition Algorithm for Radiation Diffusion Equations on Non-matching Grids

Li Yin*, Jiming Wu, and Zihuan Dai

*Institute of Applied Physics and Computational Mathematics, Beijing 100088, P. R. China.*

Received 19 January 2014; Accepted (in revised version) 13 September 2014

**Abstract.** We develop a Lions domain decomposition algorithm based on a cell functional minimization scheme on non-matching multi-block grids for nonlinear radiation diffusion equations, which are described by the coupled radiation diffusion equations of electron, ion and photon temperatures. The $L^2$ orthogonal projection is applied in the Robin transmission condition of non-matching surfaces. Numerical results show that the algorithm keeps the optimal accuracy on the whole computational domain, is robust enough on distorted meshes and curved surfaces, and the convergence rate does not depend on Robin coefficients. It is a practical and attractive algorithm in applying to the two-dimensional three-temperature energy equations of Z-pinch implosion simulation.

**AMS subject classifications**: 65M06; 65M55

**Key words**: Lions domain decomposition, radiation diffusion equations, non-matching grids, Schwarz algorithm.

## 1. Introduction

Radiation transport in astrophysical phenomena and inertial confinement fusion is often modeled using a diffusion approximation. If the time scale is shorter than the equilibrium times of electron-ion and electron-photon, the radiation diffusion process needs three different temperatures in token of each element property. With three temperatures as independent variants, the equations contain heat diffusion and energy transfer between electrons, ions, and photons. They are highly nonlinear and form a strongly coupled system of parabolic differential equations. Many authors have studied the numerical solution of the radiation diffusion equations, they focus on the high

*Corresponding author. *Email address:* yinli_kitty122@sina.com (L. Yin), wu_jiming@iapcm.ac.cn (J. Wu), dai_zihuan@iapcm.ac.cn (Z. Dai)

 ©2015 Global-Science Press

https://doi.org/10.4208/nmtma.2015.m1403 Published online by Cambridge University Press

order time integration methods [17, 19] and the nonlinear iteration solution methods on rectangular meshes [10, 13, 18].

In many application fields, the radiation diffusion problem often couples with the hydrodynamics problem, and the Lagrangian method or arbitrary Lagrangian Eulerian method is often used to solve hydrodynamics problems. Due to the deformation of complicated fluid flow, computational meshes are distorted. Numerous efforts have been devoted to efficient discretization methods for diffusion problems on distorted meshes, such as the local support operator scheme (LSOM) [16] and its modern version namely the mimetic finite difference scheme (MFD) [4, 11, 14], the multi-point flux approximation scheme (MPFA) [1,6,12], the nine-point scheme [23,25], the nonlinear monotone scheme [24, 29], and the cell functional minimization scheme (CFM) [26, 27].

In the numerical simulations of the practical physical problems, complex geometric computational domain and material surface sliding may lead to non-matching grids. In the framework of finite volume method, several discretization methods for non-matching grids have been developed [2, 3, 7], these methods deal with special non-matching grids with hanging nodes or numerical errors depend on the Robin parameter. In order to keep the original finite volume accuracy, a linear rebuilding along the interface is introduced [22]. In [28], we only use the $L^2$ projection operator on non-matching multiblock grids based on a CFM scheme in each block to get excellent results for a classical linear parabolic equation. Not only the new non-matching DDM algorithm keeps the accuracy of CFM scheme, but also numerical errors are independent of the Robin parameter. Theory analysis and numerical tests are presented.

Our objective is to develop the DDM numerical algorithm presented in [28] for radiation diffusion equations with three different temperatures to handle efficiently non-matching grids. Here, we focus on the numerical errors of the whole computational domain. Do not consider the convergence of the Schwarz method for non-matching grids. Moreover, usually the additive Schwarz method is replaced by much more efficient Krylov type methods and in addition, the small enough problems can also be solved by a direct method. Our main idea is to combine the Lions domain decomposition algorithm with the cell functional minimization (CFM) scheme, while satisfying the following properties. First, as sliding blocks are considered, the discretization in one block should not depend on the grid of the adjacent block. Second, there is a simple procedure to be used in the transmission condition of non-matching surfaces. Third, the Lions domain decomposition algorithm do not lose the finite volume accuracy on the whole computational domain. Finally, the algorithm should be robust enough on the distorted meshes and curved surfaces.

The rest of the paper is organized as follows. In the next section, the simplified three temperatures diffusion equations are described. In Section 3 the Lions domain decomposition algorithm are presented. In Section 4 the CFM scheme inside a subdomain is derived. In Section 5 how to construct discrete interface data on a general

https://doi.org/10.4208/nmtma.2015.m1403 Published online by Cambridge University Press

non-matching interface is discussed. Then in Section 6 some numerical results are presented to illustrate the robustness and accuracy. Finally some conclusions are given in Section 7.

## 2. Three temperatures diffusion equations

Radiation diffusion equations of the three temperatures simplified model are described by

$$C_{ve}\frac{\partial T_e}{\partial t} + \nabla \cdot \mathbf{F}_e = \omega_{ei}(T_i - T_e) + \omega_{er}(T_r - T_e) + S_e, \tag{2.1}$$

$$C_{vi}\frac{\partial T_i}{\partial t} + \nabla \cdot \mathbf{F}_i = \omega_{ei}(T_e - T_i) + S_i, \tag{2.2}$$

$$C_{vr}\frac{\partial T_r}{\partial t} + \nabla \cdot \mathbf{F}_r = \omega_{er}(T_e - T_r) + S_r, \tag{2.3}$$

where $T_\alpha$, $\alpha = e, i, r$, denotes the electron, ion and photon temperatures, respectively. $\omega_{ei}$ is the energy transfer coefficient between electron and ion, and $\omega_{er}$ is the energy transfer coefficient between electron and photon. $C_{v\alpha}$ is the heat capacity of each temperature and $S_\alpha$ is the corresponding source term. In practical numerical simulations, parameters $C_{v\alpha}$, $S_\alpha$, $\omega_{ei}$ and $\omega_{er}$ possibly depend on temperatures. $\mathbf{F}_\alpha$ is heat flux, which takes the form

$$\mathbf{F}_\alpha = -\kappa(T_\alpha)\nabla T_\alpha \qquad \alpha = e, i, r$$

in which $\kappa(T_\alpha)$ is the heat conduction coefficient. The computational domain is $\Omega \times [0, T]$, where $\Omega$ is a two dimensional bounded domain. The initial and boundary conditions are as follows, for $\alpha = e, i, r$

$$T_\alpha|_{t=0} = T_\alpha^0(x, y), \quad (x, y) \in \Omega, \tag{2.4}$$

$$T_\alpha(x, y, t) = g_\alpha(x, y, t), \quad (x, y) \in \partial\Omega. \tag{2.5}$$

For simplicity of descriptions, the Dirichlet boundary is used here. However, a general boundary condition also can be used.

## 3. Lions domain decomposition

The domain $\Omega$ is decomposed into $N$ non-overlapping subdomains $\Omega_j$, such that $\overline{\Omega} = \cup_{j\in\mathcal{I}}\overline{\Omega}_j$ with $\Omega_j \cap \Omega_k = \emptyset$ and the set $\mathcal{I} = \{j \in \mathbb{N} \,|\, 1 \le j \le N\}$. For all $j \in \mathcal{I}$, denote $\mathcal{V}_j = \{k \in \mathcal{I} \,|\, j \ne k \text{ and } \dim(\overline{\Omega}_j \cap \overline{\Omega}_k) = 1\}$ and for all $k \in \mathcal{V}_j$, denote $\Gamma_{jk} = \overline{\Omega}_j \cap \overline{\Omega}_k$ being an interface. At the spacial continuous level, the above problem (2.1)-(2.5) can be reformulated as the following additive Schwarz method solving Lions domain

https://doi.org/10.4208/nmtma.2015.m1403 Published online by Cambridge University Press

decomposition problem, for all $j \in \mathcal{I}$,

$$(C_{ve})_j^{n+1,s}\frac{(T_e)_j^{n+1,s}-(T_e)_j^{n,s}}{\triangle t}+\nabla\cdot(\mathbf{F}_e)_j^{n+1,s}=(\omega_{ei})_j^{n+1,s}[(T_i)_j^{n+1,s}-(T_e)_j^{n+1,s}]$$
$$+(\omega_{er})_j^{n+1,s}[(T_r)_j^{n+1,s}-(T_e)_j^{n+1,s}]+(S_e)_j^{n+1,s}\quad \text{in } \Omega_j, \tag{3.1}$$

$$(C_{vi})_j^{n+1,s}\frac{(T_i)_j^{n+1,s}-(T_i)_j^{n,s}}{\triangle t}+\nabla\cdot(\mathbf{F}_i)_j^{n+1,s}=(\omega_{ei})_j^{n+1,s}[(T_e)_j^{n+1,s}-(T_i)_j^{n+1,s}]$$
$$+(S_i)_j^{n+1,s}\quad \text{in } \Omega_j, \tag{3.2}$$

$$(C_{vr})_j^{n+1,s}\frac{(T_r)_j^{n+1,s}-(T_r)_j^{n,s}}{\triangle t}+\nabla\cdot(\mathbf{F}_r)_j^{n+1,s}=(\omega_{er})_j^{n+1,s}[(T_e)_j^{n+1,s}-(T_r)_j^{n+1,s}]$$
$$+(S_r)_j^{n+1,s}\quad \text{in } \Omega_j, \tag{3.3}$$

$$(T_\alpha)_j^{n+1,s}=g_\alpha(\cdot,\cdot,t^{n+1})\quad \alpha=e,i,r\quad \text{on } \partial\Omega\cap\partial\Omega_j, \tag{3.4}$$

$$\lambda(T_\alpha)_j^{n+1,s}+(\mathbf{F}_\alpha)_j^{n+1,s}\cdot\mathbf{n}_j=(B_\alpha)_k^{n+1,s-1}\quad \alpha=e,i,r\quad \text{on } \Gamma_{jk},\ \forall\, k\in\mathcal{V}_j, \tag{3.5}$$

$$(T_\alpha)_j^0=T_\alpha^0(\cdot,\cdot)\quad \alpha=e,i,r\quad \text{in } \Omega_j, \tag{3.6}$$

where the superscript $n$ denotes the time level, and $s$ denotes the index of subdomain iterations. Positive coefficient $\lambda$ is the Robin parameter, $\mathbf{n}_j$ denotes the unit outward normal of subdomain $\Omega_j$ along the interface $\Gamma_{jk}$. Exchanging information $(B_\alpha)_k^{n+1,s-1}$ on the interface coming from its neighbor subdomain $\Omega_k$, is defined by

$$(B_\alpha)_k^{n+1,s-1}=\begin{cases}\lambda(T_\alpha)_k^{n+1,s-1}-(\mathbf{F}_\alpha)_k^{n+1,s-1}\cdot\mathbf{n}_k, & s>1,\\ \lambda(T_\alpha)_k^{n}-(\mathbf{F}_\alpha)_k^{n}\cdot\mathbf{n}_k, & s=1.\end{cases} \tag{3.7}$$

The above system of (3.1)-(3.6) is a self-contained problem at the spatial continuous level on a subdomain. If a spacial discrete scheme with proper spacial discrete exchanging data of $(B_\alpha)_k^{n+1,s-1}$ on non-matching interfaces are given, (3.1)-(3.6) becomes a nonlinear algebraic system on a subdomain. The CFM discrete scheme in the subdomain and the interface condition on a general non-matching interface are present in next two sections. For simplicity of expositions, we introduce some notations.

- $\mathcal{T}_j$ is a set of closed subsets associated with subdomain $\Omega_j$ such that $\Omega_j=\cup_{K\in\mathcal{T}_j}K$, where $K$ denotes a control cell.
- $\mathcal{E}_j^{int}$ is the set of interior edges of $\mathcal{T}_j$.
- $\mathcal{E}_j^{ext}$ is the set of outer edges such that $\partial\Omega_j\cap\partial\Omega=\cup_{\sigma\in\mathcal{E}_j^{ext}}\sigma$, where $\sigma$ denotes a generic edge.

https://doi.org/10.4208/nmtma.2015.m1403 Published online by Cambridge University Press

- $\mathcal{E}_j^{fac}$ is the set of interface edges such that $\partial\Omega_j \backslash \partial\Omega = \cup_{\sigma\in\mathcal{E}_j^{fac}}\sigma$.
- $\Gamma_{jk} = \overline{\Omega}_j \cap \overline{\Omega}_k$ is the surface between subdomains $\Omega_j$ and $\Omega_k$.
- $\mathcal{E}_{j\to k} = \{\sigma \in \mathcal{E}_j^{fac} \,|\, \sigma \cap \Gamma_{jk} \neq \emptyset\}$ is the grid of $\Gamma_{jk}$ for the subdomain $\Omega_j$. Because the grids can be non-matching at the interface $\Gamma_{jk}$, thus $\mathcal{E}_{j\to k}$ is in general not identical to $\mathcal{E}_{k\to j}$.
- $\forall K \in \mathcal{T}_j$,

  $\mathcal{E}(K)$ denotes the set of edges of $K$, and $n_K$ is the edges number of $K$;

  $\mathbf{I}_K = (1, 1, \cdots, 1)^T$ is a $n_K$ sized vector;

  $\mathbf{I}_{K,\sigma}$ is a $n_K$ sized vector whose $\sigma$th entry is $1$ and the rest are all zero.

## 4. CFM scheme in the subdomain

In this section, we present the CFM spacial discrete scheme used in each subdomain. This scheme has a local stencil, leads to a symmetric positive definite linear system, and is linearity-preserving. Here, a cell local stencil property is important in our non-matching Lions domain decomposition algorithm, which ensures the discretization in one block independently of the grid of the adjacent block.

### 4.1. Construction of scheme

Firstly, introduce discrete unknowns $(T_\alpha)_K$ and $(T_\alpha)_{K,\sigma}$ to be approximations of solutions $T_\alpha$ at the cell center $\mathbf{x}_K$ and the edge midpoint $\mathbf{x}_{K,\sigma}$, as depicted in Fig. 1. Since there exists a unique midpoint for an edge and discrete solutions are required to be continuous at this point, for any cell $K \in \mathcal{T}_j$, we can thus always write

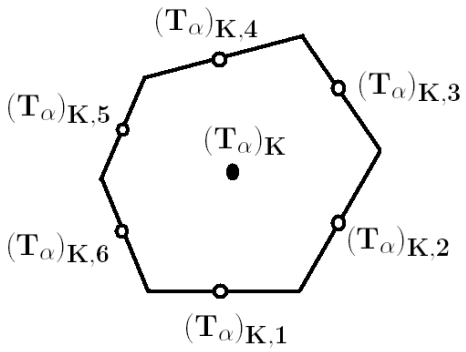



Figure 1: Locations of three temperatures.

https://doi.org/10.4208/nmtma.2015.m1403 Published online by Cambridge University Press

$$(T_\alpha)_{K,\sigma} = (T_\alpha)_{L,\sigma} = (T_\alpha)_\sigma, \quad \text{if } \sigma \in \mathcal{E}_j^{int} \text{ and } \sigma = \mathcal{E}(K) \cap \mathcal{E}(L),$$
$$(T_\alpha)_{K,\sigma} = (T_\alpha)_\sigma, \quad \text{if } \sigma \in \left(\mathcal{E}_j^{ext} \text{ or } \mathcal{E}_j^{fac}\right) \cap \mathcal{E}(K).$$

As for the heat flux, we use the notation

$$(F_\alpha)_{K,\sigma} \approx \int_\sigma \mathbf{F}_\alpha \cdot \mathbf{n}_{K,\sigma}\, ds, \quad \sigma \in \mathcal{E}(K),$$

where $\mathbf{n}_{K,\sigma}$ is the unit outward normal of the cell $K$ along $\sigma$ edge.

Secondly, minimize the following cell functional of a vector function as mentioned in [26, 27]

$$W_K(\mathbf{F}_\alpha) := \int_K \mathbf{F}_\alpha^T \Lambda_\alpha^{-1} \mathbf{F}_\alpha \, d\mathbf{x} - 2\int_K T_\alpha \,\mathrm{div}\mathbf{F}_\alpha \, d\mathbf{x} + 2\oint_{\partial K} T_\alpha \mathbf{F}_\alpha \cdot \mathbf{n}\, ds,$$

here the matrix $\Lambda_\alpha(\mathbf{x}) = \kappa(T_\alpha)\mathbb{I}$, where $\mathbb{I}$ is an $2 \times 2$ unit matrix. Numerical approximations for three terms of $W_K(\mathbf{F}_\alpha)$ are given, respectively.

$$\int_K \mathbf{F}_\alpha^T \Lambda_\alpha^{-1} \mathbf{F}_\alpha d\mathbf{x} \approx \mathbf{F}_{\alpha,K}^T \mathbb{A}_{\alpha,K} \mathbf{F}_{\alpha,K}, \tag{4.1}$$

where $\mathbf{F}_{\alpha,K} = ((F_\alpha)_{K,\sigma}, \sigma \in \mathcal{E}(K))^T$ and the $n_K \times n_K$ symmetric positive definite matrix $\mathbb{A}_{\alpha,K}$, called as cell matrix, will be specified in later.

$$\int_K T_\alpha \,\mathrm{div}\mathbf{F}_\alpha \, d\mathbf{x} \approx (T_\alpha)_K \oint_{\partial K} \mathbf{F}_\alpha \cdot \mathbf{n}\, ds \approx (T_\alpha)_K \sum_{\sigma \in \mathcal{E}(K)} (F_\alpha)_{K,\sigma}. \tag{4.2}$$

$$\oint_{\partial K} T_\alpha \mathbf{F}_\alpha \cdot \mathbf{n}\, ds \approx \sum_{\sigma \in \mathcal{E}(K)} (T_\alpha)_{K,\sigma} (F_\alpha)_{K,\sigma}. \tag{4.3}$$

Combining (4.1), (4.2) with (4.3), we get the discrete cell functional

$$W_K(\mathbf{F}_\alpha) \approx \mathbf{F}_{\alpha,K}^T \mathbb{A}_{\alpha,K} \mathbf{F}_{\alpha,K} - 2\mathbf{F}_{\alpha,K}^T \left((T_\alpha)_K \mathbf{I}_K - \mathbf{T}_{\alpha,K}\right), \tag{4.4}$$

where $\mathbf{T}_{\alpha,K} = ((T_\alpha)_{K,\sigma}, \sigma \in \mathcal{E}(K))^T$. Since $\mathbb{A}_{\alpha,K}$ is symmetric positive definite, the discrete cell functional $(4.4)$ achieves its minimum if and only if

$$\mathbb{A}_{\alpha,K} \mathbf{F}_{\alpha,K} = (T_\alpha)_K \mathbf{I}_K - \mathbf{T}_{\alpha,K}, \tag{4.5}$$

which means a consistent relation between temperature unknowns and normal heat fluxes in each cell.

At last, construct a finite volume scheme based on the relation $(4.5)$ through a cell functional minimization. By the standard finite volume spatial discretization, integrate

https://doi.org/10.4208/nmtma.2015.m1403 Published online by Cambridge University Press

$(3.1)$-$(3.3)$ on any cell $K$. Without any confusion, the superscript $s$ the index of subdomain iterations and subscript $j$ denoted $j$th subdomain are omitted. Then, we obtain equations corresponding to the cell centered unknown $(T_\alpha)_K$,

$$(C_{ve})_K^{n+1}\frac{(T_e)_K^{n+1}-(T_e)_K^n}{\triangle t}+\frac{1}{m(K)}\mathbf{I}_K^T(\mathbb{A}_{e,K}^{-1})^{n+1}\left((T_e)_K^{n+1}\mathbf{I}_K-\mathbf{T}_{e,K}^{n+1}\right)$$

$$=(\omega_{ei})_K^{n+1}\left((T_i)_K^{n+1}-(T_e)_K^{n+1}\right)+(\omega_{er})_K^{n+1}\left((T_r)_K^{n+1}-(T_e)_K^{n+1}\right)+(S_e)_K^{n+1}, \tag{4.6}$$

$$(C_{vi})_K^{n+1}\frac{(T_i)_K^{n+1}-(T_i)_K^n}{\triangle t}+\frac{1}{m(K)}\mathbf{I}_K^T(\mathbb{A}_{i,K}^{-1})^{n+1}\left((T_i)_K^{n+1}\mathbf{I}_K-\mathbf{T}_{i,K}^{n+1}\right)$$

$$=(\omega_{ei})_K^{n+1}\left((T_e)_K^{n+1}-(T_i)_K^{n+1}\right)+(S_i)_K^{n+1}, \tag{4.7}$$

$$(C_{vr})_K^{n+1}\frac{(T_r)_K^{n+1}-(T_r)_K^n}{\triangle t}+\frac{1}{m(K)}\mathbf{I}_K^T(\mathbb{A}_{r,K}^{-1})^{n+1}\left((T_r)_K^{n+1}\mathbf{I}_K-\mathbf{T}_{r,K}^{n+1}\right)$$

$$=(\omega_{er})_K^{n+1}\left((T_e)_K^{n+1}-(T_r)_K^{n+1}\right)+(S_r)_K^{n+1}, \tag{4.8}$$

where $(4.5)$ are used and $m(K)$ is the measure of cell $K$. The discrete equation corresponding to an interior edge $\sigma\in\mathcal{E}_j^{int}$ and $\sigma=\mathcal{E}(K)\cap\mathcal{E}(L)$ is obtained by using the continuity of the flux, i.e., $(F_\alpha)_{K,\sigma}^{n+1}+(F_\alpha)_{L,\sigma}^{n+1}=0$. Specifically, we have

$$\mathbf{I}_{K,\sigma}^T(\mathbb{A}_{\alpha,K}^{-1})^{n+1}\left((T_\alpha)_K^{n+1}\mathbf{I}_K-\mathbf{T}_{\alpha,K}^{n+1}\right)=\mathbf{I}_{L,\sigma}^T(\mathbb{A}_{\alpha,L}^{-1})^{n+1}\left(\mathbf{T}_{\alpha,L}^{n+1}-(T_\alpha)_L^{n+1}\mathbf{I}_L\right). \tag{4.9}$$

For an edge $\sigma\in\mathcal{E}_j^{ext}$ on the boundary $\partial\Omega$, integrating $(3.4)$ on $\sigma$ and the corresponding edge values can be obtained,

$$(T_\alpha)_\sigma^{n+1}=\frac{1}{m(\sigma)}\int_\sigma g_\alpha(\cdot,\cdot,t^{n+1})\,ds,\quad \alpha=e,i,r. \tag{4.10}$$

For an interface edge $\sigma\in\mathcal{E}_j^{fac}\cap\mathcal{E}(K)$ on the interface boundary $\mathcal{E}_{j\to k}$, integrating $(3.5)$ on $\sigma$ and the corresponding equation analogously can be written as

$$\lambda(T_\alpha)_\sigma^{n+1,s}+\frac{1}{m(\sigma)}\mathbf{I}_{K,\sigma}^T(\mathbb{A}_{\alpha,K}^{-1})^{n+1,s}\left((T_\alpha)_K^{n+1,s}\mathbf{I}_K-\mathbf{T}_{\alpha,K}^{n+1,s}\right)=(B_\alpha)_{k,\sigma}^{n+1,s-1}, \tag{4.11}$$

where the superscript $s$ the index of subdomain iterations are specified, because of difference on two sides. The right term of $(4.11)$ is an approximation of $(s-1)$th exchanging information coming from the neighbor subdomain $\Omega_k$ on the interface edge $\sigma$, which will be discussed in details in another section for a general non-matching interface.

## 4.2. Subdomain linear system

Full discrete Eqs. $(4.6)$-$(4.11)$ lead to a nonlinear algebraic system on a subdomain. There are many iterative methods to solve the nonlinear algebraic system, such as

https://doi.org/10.4208/nmtma.2015.m1403 Published online by Cambridge University Press

Picard iterative method, or a partial Newton iterative method. This is not the important part in this article, but we want to point out that exchanging information on subdomain interfaces and the nonlinear iteration will happen at the same time in our Lions domain decomposition algorithm. In order to give a clear and complete non-matching Lions domain decomposition algorithm for radiation diffusion equations, here we give the following linear system on a subdomain by Picard iterative method.

$$
\begin{aligned}
&(C_{ve})_K^{n+1,s-1}\frac{(T_e)_K^{n+1,s}-(T_e)_K^n}{\triangle t}+\frac{1}{m(K)}\mathbf{I}_K^T(\mathbb{A}_{e,K}^{-1})^{n+1,s-1}\left((T_e)_K^{n+1,s}\mathbf{I}_K-\mathbf{T}_{e,K}^{n+1,s}\right)\\
=\ &(\omega_{ei})_K^{n+1,s-1}\left((T_i)_K^{n+1,s}-(T_e)_K^{n+1,s}\right)+(\omega_{er})_K^{n+1,s-1}\left((T_r)_K^{n+1,s}-(T_e)_K^{n+1,s}\right)\\
&\quad+(S_e)_K^{n+1,s-1},\qquad \forall K\in\mathcal{T}_j\\
&(C_{vi})_K^{n+1,s-1}\frac{(T_i)_K^{n+1,s}-(T_i)_K^n}{\triangle t}+\frac{1}{m(K)}\mathbf{I}_K^T(\mathbb{A}_{i,K}^{-1})^{n+1,s-1}\left((T_i)_K^{n+1,s}\mathbf{I}_K-\mathbf{T}_{i,K}^{n+1,s}\right)\\
=\ &(\omega_{ei})_K^{n+1,s-1}\left((T_e)_K^{n+1,s}-(T_i)_K^{n+1,s}\right)+(S_i)_K^{n+1,s-1},\qquad \forall K\in\mathcal{T}_j\\
&(C_{vr})_K^{n+1,s-1}\frac{(T_r)_K^{n+1,s}-(T_r)_K^n}{\triangle t}+\frac{1}{m(K)}\mathbf{I}_K^T(\mathbb{A}_{r,K}^{-1})^{n+1,s-1}\left((T_r)_K^{n+1,s}\mathbf{I}_K-\mathbf{T}_{r,K}^{n+1,s}\right)\\
=\ &(\omega_{er})_K^{n+1,s-1}\left((T_e)_K^{n+1,s}-(T_r)_K^{n+1,s}\right)+(S_r)_K^{n+1,s-1},\qquad \forall K\in\mathcal{T}_j
\end{aligned}
$$

$$
\begin{aligned}
&\mathbf{I}_{K,\sigma}^T(\mathbb{A}_{\alpha,K}^{-1})^{n+1,s-1}\left((T_\alpha)_K^{n+1,s}\mathbf{I}_K-\mathbf{T}_{\alpha,K}^{n+1,s}\right)=\mathbf{I}_{L,\sigma}^T(\mathbb{A}_{\alpha,L}^{-1})^{n+1,s-1}\\
&\left(\mathbf{T}_{\alpha,L}^{n+1,s}-(T_\alpha)_L^{n+1,s}\mathbf{I}_L\right),\quad \forall\sigma\in\mathcal{E}_j^{int}\text{ and }\sigma=\mathcal{E}(K)\cap\mathcal{E}(L),\ \alpha=e,i,r\\
&\lambda(T_\alpha)_\sigma^{n+1,s}+\frac{1}{m(\sigma)}\mathbf{I}_{K,\sigma}^T(\mathbb{A}_{\alpha,K}^{-1})^{n+1,s-1}\left((T_\alpha)_K^{n+1,s}\mathbf{I}_K-\mathbf{T}_{\alpha,K}^{n+1,s}\right)=(B_\alpha)_{k,\sigma}^{n+1,s-1},\\
&\qquad\forall\sigma=\mathcal{E}_j^{fac}(K)\cap\mathcal{E}_{j\to k},\ \alpha=e,i,r\\
&(T_\alpha)_\sigma^{n+1,s}=\frac{1}{m(\sigma)}\int_\sigma g_\alpha(\cdot,\cdot,t^{n+1})\,ds,\qquad \forall\,\sigma=\mathcal{E}_j^{ext},\ \alpha=e,i,r
\end{aligned}
$$

where

$$
C_{v\alpha}^{n+1,s-1}=\begin{cases}C_{v\alpha}(t^{n+1},T_\alpha^{n+1,s-1}), & s>1,\\ C_{v\alpha}(t^{n+1},T_\alpha^n), & s=1.\end{cases}
$$

https://doi.org/10.4208/nmtma.2015.m1403 Published online by Cambridge University Press

and other parameters $S_\alpha^{n+1,s-1}$, $\omega_{ei}^{n+1,s-1}$ and $\omega_{er}^{n+1,s-1}$ are similar. The superscripts $n+1$ and $n$ denote the time levels $t^{n+1}$ and $t^n$. Since information between subdomains exchanges at the nonlinear iteration, thus the superscript $s$ is the nonlinear and subdomains iteration index.

Let $\mathbf{T}$ be a vector composed of unknowns on the subdomain $\Omega_j$,

$$\mathbf{T} = ((T_e)_K, (T_i)_K, (T_r)_K, \cdots, (T_e)_\sigma, (T_i)_\sigma, (T_r)_\sigma, \cdots),$$

where all cell center unknowns are arranged in front, and all cell edge unknowns are in latter positions. Both $K \in \mathcal{T}_j$ and $\sigma \in \mathcal{E}_j^{int} \cup \mathcal{E}_j^{fac}$ are arranged in a sequence. Similar definitions of vectors for the source term and the interface exchanging term, with the same length of $\mathbf{T}$, are given by

$$\mathbf{S} = ((S_e)_K, (S_i)_K, (S_r)_K, \cdots, 0, 0, 0, \cdots),$$

$$\mathbf{B} = (0, 0, 0, \cdots, (B_e)_\sigma, (B_i)_\sigma, (B_r)_\sigma, \cdots),$$

For the source vector $\mathbf{S}$, their elements are zeros except corresponding positions of cell center unknowns. For the interface exchanging vector $\mathbf{B}$, their elements are zeros except positions of cell edge $\sigma$ on the interfaces.

If the source vector $\mathbf{S}^{n+1,s-1}$, the interface exchanging vector $\mathbf{B}^{n+1,s-1}$, $\mathbf{T}^n$ and $\mathbf{T}^{n+1,s-1}$ are known, the above linear system can be written as in the following algebra form with the coefficient matrix $\mathbb{F}(\mathbf{T}^{n+1,s-1})$

$$\mathbb{F}(\mathbf{T}^{n+1,s-1})\mathbf{T}^{n+1,s} = \mathbf{G}(\mathbf{T}^n, \mathbf{S}^{n+1,s-1}, \mathbf{B}^{n+1,s-1}). \tag{4.12}$$

Then, the above linear system (4.12) on the each subdomain can be solved by the GMRES method in parallel.

### 4.3. Construction of $\mathbb{A}_{\alpha,K}$

It remains to specify the cell matrix $\mathbb{A}_{\alpha,K}$ in (4.5) to complete the CFM scheme. Motivated by the idea of [5], we have already minutely studied constructions of the cell matrix satisfying the linearity-preserving criterion in [26]. Of course that the form of $\mathbb{A}_{\alpha,K}$ is not unique. Here, we just simply give two forms of $\mathbb{A}_{\alpha,K}$.

In constructing a symmetric positive cell matrix $\mathbb{A}_{\alpha,K}$, we can choose

$$\mathbb{A}_{\alpha,K} = \frac{1}{m(K)}\mathfrak{U}_K \Lambda_{\alpha,K}^{-1} \mathfrak{U}_K^T + \mathfrak{C}_{\alpha,K}\mathfrak{D}_K\, \mathfrak{C}_{\alpha,K}^T, \tag{4.13}$$

where $\mathfrak{D}_K$ is an arbitrary $(n_K - 2) \times (n_K - 2)$ symmetric positive definite matrix, and $\mathfrak{C}_{\alpha,K}$ is a $n_K \times (n_K - 2)$ matrix whose column vectors span the null space of the matrix $\mathfrak{F}_{\alpha,K}^T$ such that $\mathfrak{F}_{\alpha,K}^T \mathfrak{C}_{\alpha,K} = 0$. Here $\mathfrak{F}_{\alpha,K} = (f_{\sigma,j}^\alpha)$ and $\mathfrak{U}_K = (u_{\sigma,j})$ are $n_K \times 2$ matrices, whose entries are given by

$$f_{\sigma,j}^\alpha = -|\sigma|\mathbf{e}_j^T \Lambda_{\alpha,K}\mathbf{n}_{K,\sigma}, \quad u_{\sigma,j} = \mathbf{e}_j^T(\mathbf{x}_K - \mathbf{x}_{K,\sigma}),$$

https://doi.org/10.4208/nmtma.2015.m1403 Published online by Cambridge University Press

here $\mathbf{e}_1 = (1,0)^T,\ \mathbf{e}_2 = (0,1)^T$. Since the inverse matrix of the cell matrix is needed in computation, the direct construction of $\mathbb{A}^{-1}_{\alpha,K}$ can be written as

$$\mathbb{A}^{-1}_{\alpha,K} = \frac{1}{m(K)}\mathfrak{F}_{\alpha,K}\Lambda^{-1}_{\alpha,K}\mathfrak{F}^T_{\alpha,K} + \widetilde{\mathfrak{C}}_K\widetilde{\mathfrak{D}}_K\,\widetilde{\mathfrak{C}}^T_K, \tag{4.14}$$

where $\widetilde{\mathfrak{C}}_K$ be an $n_K \times (n_K - 2)$ matrix whose column vectors span the null space of the matrix $\mathfrak{U}^T_K$ such that $\mathfrak{U}^T_K\widetilde{\mathfrak{C}}_K = 0$, and $\widetilde{\mathfrak{D}}_K$ denotes an arbitrary $(n_K - 2) \times (n_K - 2)$ symmetric positive definite matrix.

**Remark 4.1.** Both $\mathfrak{D}_K$ in (4.13) and $\widetilde{\mathfrak{D}}_K$ in (4.14) are arbitrary $(n_K - 2) \times (n_K - 2)$ symmetric positive definite matrixes. In practical computations, we always choose them to be identity matrixes.

## 5. Construction of discrete data on non-matching interfaces

For a general non-matching interface, the important key is how to impose continuity of temperatures and of normal heat fluxes across non-matching interfaces. Whatever structured or unstructured meshes on the subdomains, exchanging information on the interface in the two-dimensional space domain leads to a one-dimensional problem. Let $n_{j\to k}$ and $n_{k\to j}$ be the numbers of cell edges of the interface $\mathcal{E}_{j\to k}$ and $\mathcal{E}_{k\to j}$, respectively. Since the CFM discrete scheme has approximate temperatures on the midpoint of cell edges, the key of exchanging interface information from subdomain $\Omega_k$ to $\Omega_j$ is how to construct $n_{j\to k}$ vector data on surface grids $\mathcal{E}_{j\to k}$ from $n_{k\to j}$ vector data on surface grids $\mathcal{E}_{k\to j}$, see Fig. 2.

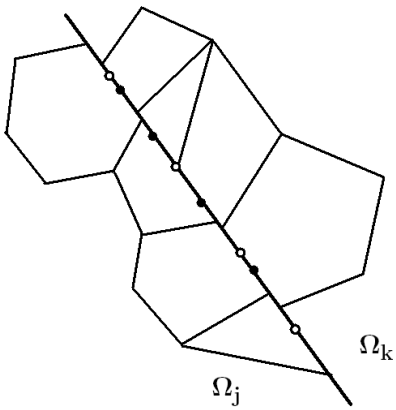



Figure 2: A part of non-matching surface $\Gamma_{jk} = \overline{\Omega}_j \cap \overline{\Omega}_k$: empty circle denotes the midpoint of edge $\sigma^j \in \mathcal{E}_{j\to k}$, and solid circle denotes the midpoint of edge $\sigma^k \in \mathcal{E}_{k\to j}$.

By using the relation (4.5) in the CFM discrete scheme, exchanging information $(B_\alpha)^{n+1,s-1}_k$ (defined by (3.7)) from the subdomain $\Omega_k$ in the Lions domain decomposition algorithm can be rewritten as the discrete vector $(\mathbf{B}_\alpha)^{n+1,s-1}_k = \left(b^{n+1,s-1}_{\alpha,\sigma^k}\right)_{n_{k\to j}}$.

https://doi.org/10.4208/nmtma.2015.m1403 Published online by Cambridge University Press

The element $b^{n+1,s-1}_{\alpha,\sigma^k}$ is defined by, for $\sigma^k \in \mathcal{E}_{k\to j} \cap \mathcal{E}(K)$, where $K \in \mathcal{T}_k$

$$\lambda(T_\alpha)^{n+1,s-1}_{\sigma^k} + \frac{1}{m(\sigma^k)}\mathbf{I}^T_{K,\sigma^k}(\mathbb{A}^{-1}_{\alpha,K})^{n+1,s-1}\left((T_\alpha)^{n+1,s-1}_K\mathbf{I}_K - \mathbf{T}^{n+1,s-1}_{\alpha,K}\right), \quad s>1,$$

$$\lambda(T_\alpha)^{n}_{\sigma^k} + \frac{1}{m(\sigma^k)}\mathbf{I}^T_{K,\sigma^k}(\mathbb{A}^{-1}_{\alpha,K})^{n}\left((T_\alpha)^{n}_K\mathbf{I}_K - \mathbf{T}^{n}_{\alpha,K}\right), \quad s=1.$$

Next, for any surface edge $\sigma \in \mathcal{E}_{j\to k}$ on the boundary of subdomain $\Omega_j$, we will use discrete exchanging information vector $(\mathbf{B}_\alpha)^{n+1,s-1}_k$ coming from neighbor subdomain $\Omega_k$ to construct discrete interface data $(B_\alpha)^{n+1,s-1}_{k,\sigma}$ in the right hand side of (4.11). Introduce $P^0(\mathcal{E}_{j\to k})$ the space of piecewise constant functions on the surface grid $\mathcal{E}_{j\to k}$ and the following $L^2$ orthogonal projection.

**$L^2$ orthogonal projection** Let $P_{jk}$ be the $L^2$ orthogonal projection from $P^0(\mathcal{E}_{k\to j})$ onto $P^0(\mathcal{E}_{j\to k})$. For $v_k \in P^0(\mathcal{E}_{k\to j})$ and $\sigma^j \in \mathcal{E}_{j\to k}$, it is defined by

$$[P_{jk}(v_k)]_{\sigma^j} = \frac{1}{m(\sigma^j)}\int_{\sigma^j} v_k\, ds = \sum_{\sigma^k\in\mathcal{E}_{k\to j}} \frac{m(\sigma^j\cap\sigma^k)}{m(\sigma^j)} v_{k,\sigma^k}. \tag{5.1}$$

The corresponding matrix $\mathbb{P} = \{p_{ab}\}_{n_{j\to k}\times n_{k\to j}}$ of the $L^2$ orthogonal projection operator $P_{jk}$ is given by

$$p_{ab} = \frac{m(\sigma^j_a \cap \sigma^k_b)}{m(\sigma^j_a)}.$$

Then, for a general non-matching surface, the discrete exchanging information $(B_\alpha)^{n+1,s-1}_{k,\sigma}$ in (4.11), is constructed by

$$(B_\alpha)^{n+1,s-1}_{k,\sigma} = \left[P_{jk}\left((\mathbf{B}_\alpha)^{n+1,s-1}_k\right)\right]_\sigma, \tag{5.2}$$

where $(\mathbf{B}_\alpha)^{n+1,s-1}_k$ is a $n_{k\to j}$ vector coming from neighbor subdomain $\Omega_k$, as presented above. Only $L^2$ orthogonal projection operator is applied in the transmission condition (4.11) with (5.2), this is a relatively simple procedure dealing with non-matching surface.

## 6. Numerical results

In this section, some numerical results are tested to show the Lions domain decomposition algorithm for the three temperatures diffusion equations do not lose the accuracy on multi-blocks with non-matching surfaces, and it robust enough on the distorted meshes and curved surfaces.

https://doi.org/10.4208/nmtma.2015.m1403 Published online by Cambridge University Press

In order to test the accuracy of the algorithm on the whole computing domain, for numerical solutions $T_\alpha^h = \{(T_\alpha)_K, (T_\alpha)_{K,\sigma}\}$, discrete norms in $L^2$ and $H^1$ are respectively defined by

$$\|T_\alpha^h\|_{L^2(\Omega)}(t) = \left(\sum_{j\in\mathcal{I}}\sum_{K\in\mathcal{T}_j} m(K)(T_\alpha)_K^2(t)\right)^{1/2},$$

$$\|T_\alpha^h\|_{H^1(\Omega)\times L^2[0,T]} = \left(\sum_{k=1}^{n}\sum_{j\in\mathcal{I}}\sum_{K\in\mathcal{T}_j} \|\mathbb{Q}_K^{1/2}(T_\alpha)_K(t^k)\mathbf{I}_K - \mathbf{T}_{\alpha,K}(t^k)\|^2\triangle t\right)^{1/2},$$

where $\mathbb{Q}_K$ is a $n_K\times n_K$ diagonal matrix associated with the cell $K$ whose nonzero entry in the $i$th row is $m(\sigma_i)/d_i$, $m(\sigma_i)$ is the measure of $i$th edge $\sigma_i$, and $d_i$ is the distance between the cell center of $K$ and the $i$th edge's midpoint. Then, approximate solution errors in $L^2$ and $H^1$ discrete norms are given by

$$E_\alpha^{L^2}(h,t) = \|T_\alpha^h - \Pi^h T_\alpha\|_{L^2(\Omega)}(t),$$

$$E_\alpha^{H^1}(h) = \|T_\alpha^h - \Pi^h T_\alpha\|_{H^1(\Omega)\times L^2[0,T]},$$

where $\Pi^h T_\alpha = \{T_\alpha(\mathbf{x}_K), T_\alpha(\mathbf{x}_{K,\sigma})\}$ is the interpolation function of exact solution $T_\alpha$, $\mathbf{x}_K$ and $\mathbf{x}_{K,\sigma}$ denote the cell center and the edge midpoint, respectively. The rate of convergence can be obtained on each two successive meshes by the following formula

$$R_\alpha^q = \frac{\log[E_\alpha^q(h_2)/E_\alpha^q(h_1)]}{\log(h_2/h_1)}, \quad \alpha = e,i,r, \quad q = L^2, H^1.$$

In computing numerical tests, we directly use the construction form (4.14) to get the inverse of the cell matrix, choose $\widetilde{\mathfrak{D}}_K$ to be an identity matrix, and employ the geometric center as the cell center. Throughout, we use GMRES method [21] to solve the linear systems in all experiments.

## 6.1. Test problem 1

Parameters in the three temperatures diffusion model of (2.1)-(2.3) are specified by

$$\omega_{er} = T_e, \quad \omega_{ei} = T_i^3,$$

$$C_{v\alpha} = 1 + T_\alpha^2, \quad S_\alpha = 1 - 50T_\alpha + T_\alpha^2, \quad \kappa(T_\alpha) = 1 + T_\alpha^2, \quad \alpha = e,i,r.$$

The whole computing domain is given by $\Omega = (0,1)\times(0,1)$, and the associated analytical solutions are

$$T_\alpha = t + 3x + 4y + 1, \quad \alpha = e,i,r.$$

https://doi.org/10.4208/nmtma.2015.m1403 Published online by Cambridge University Press

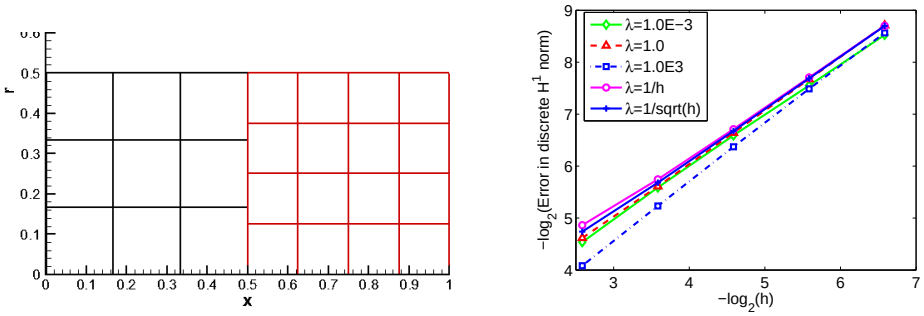



Figure 3: (a) Two-subdomain decomposition on non-matching Cartesian meshes. (b) Log of the error $H^1$ norm vs. log of the mesh size $(\mathrm{h})$.

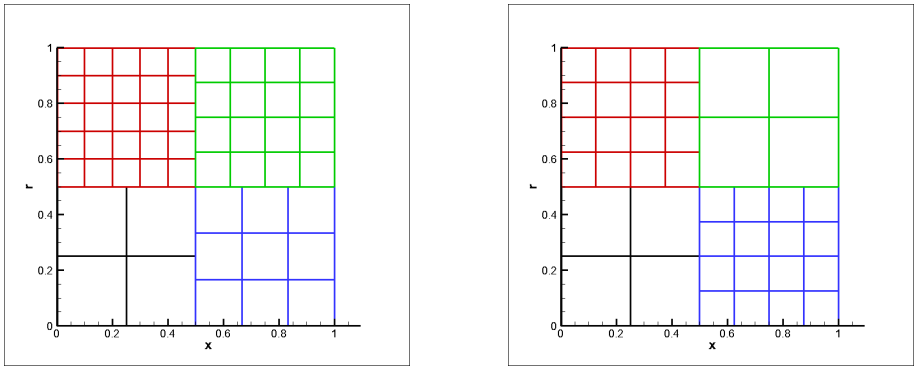



Figure 4: 1-level non-matching Cartesian meshes. $(a)$ a general case. $(b)$ a special case.

The stopping criterion of the Lions domain decomposition algorithm is that the max norm of jumps of the each local subdomain solution is smaller than $10^{-6}$ with the time step $\triangle t = 10^{-7}$ and the final time $T = 0.01$.

**A wide range of values for Robin coefficients**. We test a two-subdomain decomposition (see Fig. 3(a)) with a wide range of values for Robin coefficients to study the dependency of the error estimate in discrete $H^1$-norm for Robin coefficients. Fig. 3(b) gives the asymptotic behavior of the log of the error as a function of the log of the mesh size $h$ for different Robin coefficients $\lambda = 10^{-3}$, 1.0, $10^3$, $h^{-1}$, $h^{-1/2}$. We observe that numerical errors do not depend on Robin interface coefficients, and for a wide range of Robin coefficients an order of 1.0 in discrete $H^1$ norm is obtained as what is expected. Since the Robin coefficient does not affect the numerical accuracy, we choose it to be a constant $10^3$ in the following computational tests.

**A general non-matching surface case**. We cut the domain $\Omega$ into four non-overlapping subdomains $\Omega_1 = (0, 1/2) \times (0, 1/2)$, $\Omega_2 = (1/2, 1) \times (0, 1/2)$, $\Omega_3 = (0, 1/2) \times (1/2, 1)$ and $\Omega_4 = (1/2, 1) \times (1/2, 1)$ with a corner and four straight line surfaces. Four subdomains are partitioned by regular Cartesian meshes. Here, computations are tested on two kinds of non-matching surfaces as shown in Fig. 4. One kind of interface meshes is an arbitrary non-matching grids which is a general non-matching

https://doi.org/10.4208/nmtma.2015.m1403 Published online by Cambridge University Press

Table 1: Numerical results on non-matching meshes as shown in Fig.4(a).

| mesh | $E_e^{L^2}(h,T)$ | $R_e^{L^2}$ | $E_e^{H^1}(h)$ | $R_e^{H^1}$ |
|---|---|---|---|---|
| 1-level | 3.6984E-2 | * | 1.0672E-1 | * |
| 2-level | 1.3361E-2 | 1.47 | 5.0473E-2 | 1.08 |
| 3-level | 3.5170E-3 | 1.93 | 2.3927E-2 | 1.08 |
| 4-level | 8.5927E-4 | 2.03 | 1.1067E-2 | 1.11 |

Table 2: Numerical results on non-matching meshes as shown in Fig.4(b).

| mesh | $E_e^{L^2}(h,T)$ | $R_e^{L^2}$ | $E_e^{H^1}(h)$ | $R_e^{H^1}$ |
|---|---|---|---|---|
| 1-level | 3.8422E-2 | * | 1.0188E-1 | * |
| 2-level | 1.2939E-2 | 1.57 | 5.7257E-2 | 0.83 |
| 3-level | 3.4941E-3 | 1.89 | 3.0759E-2 | 0.90 |
| 4-level | 8.7418E-4 | 2.00 | 1.5410E-2 | 1.00 |
| 5-level | 2.1040E-4 | 2.05 | 7.1910E-3 | 1.10 |

case, and the other is nested grids on the interface which is a special non-matching case. In order to test the convergence order, computational errors are obtained on a series of refined such Cartesian non-matching meshes. Numerical results of the electron temperature are presented in Table 1 and Table 2, results of ion and photon temperatures are omitted, which are similar with electron temperature. The convergence rates of algorithm for numerical errors in discrete $L^2$ and $H^1$ norms are about $h^2$ and $h^1$ respectively.

**A curved non-matching surface case**. Non-orthogonal meshes always appear in the arbitrary Lagrangian-Eulerian hydrodynamics algorithms. Material surfaces can be distorted in practical problem of coupled radiation diffusion and hydrodynamics calculations. Now, we consider non-matching surfaces are curves, such as shown in Fig. 5. Here, the random quadrilateral mesh is constructed from the uniform square mesh with the mesh size $h$ by random distortion of its nodes:

$$x := x + 2\alpha\xi_x h, \quad y := y + 2\alpha\xi_y h, \tag{6.1}$$

where $\xi_x$ and $\xi_y$ are random variales with values between $-0.5$ and $0.5$ and $\alpha \in [0, 0.5]$ is the degree of distortion. The larger $\alpha$ is, the more distorted mesh is produced. If $\alpha > 0.25$, mesh cells may be non-convex. While, our CFM scheme can deal with some concave cells, and the corresponding theorem analysis has been proven in [26]. The domain $\Omega$ is decomposed into four subdomains with a corner and four curved non-matching surfaces. Four subdomains are partitioned by random meshes with random disturbance $\alpha = 0.3$ in definition $(6.1)$, which leads to a non-smooth and non-matching curved surfaces as present in Fig. 5(a). Numerical results are given in Table 3. Similarly, when subdomains are partitioned by sine meshes, non-matching surfaces are smooth curves as depicted in Fig. 5(b), and corresponding numerical results are present in Table 4. On these distorted meshes with non-matching curved surfaces, the convergence

https://doi.org/10.4208/nmtma.2015.m1403 Published online by Cambridge University Press

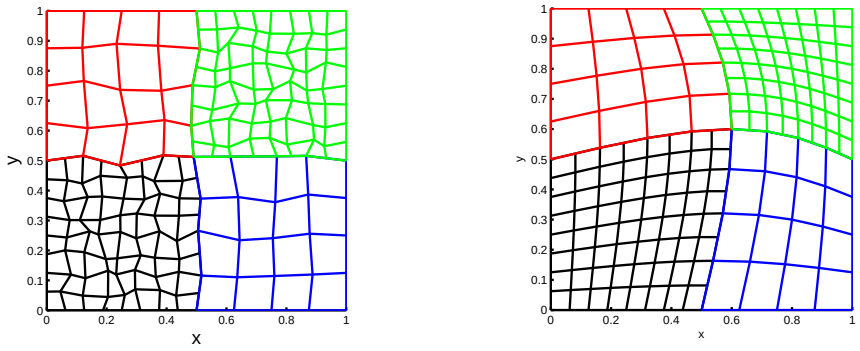



Figure 5: Curved non-matching surface case. $(a)$ random mesh with non-smooth curved surfaces. $(b)$ sine mesh with smooth curved surfaces.

Table 3: Numerical results on random meshes with non-matching and non-smooth curved surfaces.

| mesh | $E_e^{L^2}(h,T)$ | $R_e^{L^2}$ | $E_e^{H^1}(h)$ | $R_e^{H^1}$ |
|---|---|---|---|---|
| 1-level | 3.8444E-2 | * | 9.9561E-2 | * |
| 2-level | 1.3211E-2 | 1.54 | 5.7332E-2 | 0.80 |
| 3-level | 3.5708E-3 | 1.89 | 3.2607E-2 | 0.81 |
| 4-level | 8.7422E-4 | 2.03 | 1.5871E-2 | 1.04 |
| 5-level | 2.1291E-4 | 2.04 | 7.4870E-3 | 1.08 |

Table 4: Numerical results on sine meshes with non-matching and smooth curved surfaces.

| mesh | $E_e^{L^2}(h,T)$ | $R_e^{L^2}$ | $E_e^{H^1}(h)$ | $R_e^{H^1}$ |
|---|---|---|---|---|
| 1-level | 4.8795E-2 | * | 1.1467E-1 | * |
| 2-level | 1.7403E-2 | 1.49 | 6.7653E-2 | 0.76 |
| 3-level | 5.0278E-3 | 1.79 | 3.8668E-2 | 0.81 |
| 4-level | 1.3206E-3 | 1.93 | 1.9907E-2 | 0.96 |
| 5-level | 3.3906E-4 | 1.96 | 9.3811E-3 | 1.09 |

rates for numerical errors in discrete $L^2$ and $H^1$ norms also can reach second order and first order, respectively.

Numerical tests show that our Lions domain decomposition algorithm do not lose the finite volume accuracy on the whole computational domain with arbitrary non-matching surfaces, and it is robust enough to get optimal convergence rates even on the distorted meshes with curved surfaces.

## 6.2. Test problem 2

Magnetics Atom Radiation Electron Dynamics (MARED) code, which is a two dimensional, three temperature, radiation magnetohydrodynamic Lagrangian code, is developed for the Z-pinch implosion simulation [30]. In this simulation program, the

https://doi.org/10.4208/nmtma.2015.m1403 Published online by Cambridge University Press

two-dimensional three-temperature energy equations are described by

$$C_{ve}\frac{\partial T_e}{\partial t}+\left(P_e+\frac{\partial \varepsilon_e}{\partial V}\right)\frac{\partial V}{\partial t}+V\nabla\cdot\mathbf{F}_e=\omega_{ei}(T_i-T_e)+\omega_{er}(T_r-T_e), \quad (6.2)$$

$$C_{vi}\frac{\partial T_i}{\partial t}+\left(P_i+q_i+\frac{\partial \varepsilon_i}{\partial V}\right)\frac{\partial V}{\partial t}+V\nabla\cdot\mathbf{F}_i=\omega_{ei}(T_e-T_i), \quad (6.3)$$

$$C_{vr}\frac{\partial T_r}{\partial t}+\left(P_r+\frac{\partial \varepsilon_r}{\partial V}\right)\frac{\partial V}{\partial t}+V\nabla\cdot\mathbf{F}_r=\omega_{er}(T_e-T_r), \quad (6.4)$$

where $\varepsilon_\alpha=\varepsilon_\alpha(\rho,T_\alpha)$ is energy of unit mass, $P_\alpha$ is pressure, $V=1/\rho$ is specific volume, $\rho$ is material density, $q_i$ is an artificial viscosity term, and heat flux $\mathbf{F}_\alpha$ takes the form

$$\mathbf{F}_\alpha=-\kappa_\alpha(\rho,T_\alpha)\nabla T_\alpha \qquad \alpha=e,i,r.$$

In the computation Test 2, corresponding parameters such as energy transfer coefficients $\omega_{ei}$, $\omega_{er}$, and $C_{v\alpha}$, all deduced from MARED code of simulating practical physical problems. Since computational parameters of real problem are so complicated, here we can only give the approximate order of the nonlinear heat conduction coefficients $\kappa_\alpha=O(T_\alpha^{5/2})$, $\alpha=e,i$, and $\kappa_r=O(T_r^3)$. In order to keep the propagation velocity of a radiation wave front in a vacuum less than the speed of light, we also use the flux limiter technology [20] in the computation of heat flux in this test. The practical computing domain is a 2cm square with $(x,y)\in\Omega=(0,2*10^4)\times(0,2*10^4)\mu$m. Boundary conditions are as follows.

$$\mathbf{F}_\alpha\cdot\mathbf{n}|_{x=0}=\mathbf{F}_\alpha\cdot\mathbf{n}|_{x=2*10^4}=\mathbf{F}_\alpha\cdot\mathbf{n}|_{y=0}=0, \quad \alpha=e,i,r, \quad (6.5)$$

where $\mathbf{n}$ is the unit normal of the boundary, and the top boundary is free surface is defined by

$$\mathbf{F}_e\cdot\mathbf{n}|_{y=2*10^4}=\mathbf{F}_i\cdot\mathbf{n}|_{y=2*10^4}=0, \quad T_r(x,y,t)|_{y=2*10^4}=T_r^{top}(x,y,t). \quad (6.6)$$

The initial condition is

$$T_\alpha|_{t=0}=T_\alpha^0(x,y), \quad \alpha=e,i,r. \quad (6.7)$$

The problem (6.2)-(6.4) with initial boundary conditions (6.5)-(6.7) describes temperatures diffusion from the top radiation temperature source, which is a one-dimensional physical process and numerical results should not depend on meshes. Numerical algorithm without high accuracy on distorted meshes can twist the temperatures changing process, which have been mentioned in [8]. In this test, we put one material (W) in the whole computational domain, choose $T_r^{top}=10$ millions of degrees, $T_\alpha^0$=5 millions of degrees and use non-matching sine meshes partitions as shown in Fig. 6. The corresponding numerical results of photon temperature in cell centers are present in Fig. 7. Numerical results are independent of two-dimensional meshes, non-matching surfaces and surface shapes. Our Lions domain decomposition algorithm based on CFM scheme can get truly physical images to illustrate temperatures diffusion processes.

https://doi.org/10.4208/nmtma.2015.m1403 Published online by Cambridge University Press

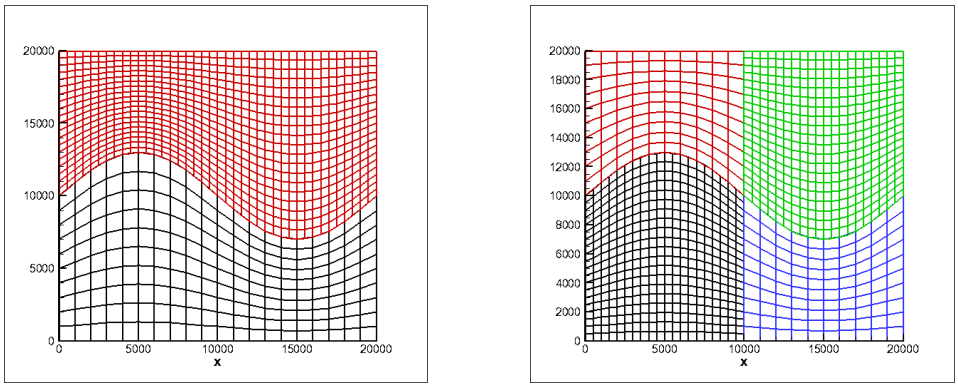



Figure 6: Non-matching sine meshes. $(a)$ Two subdomains. $(b)$ Four subdomains.

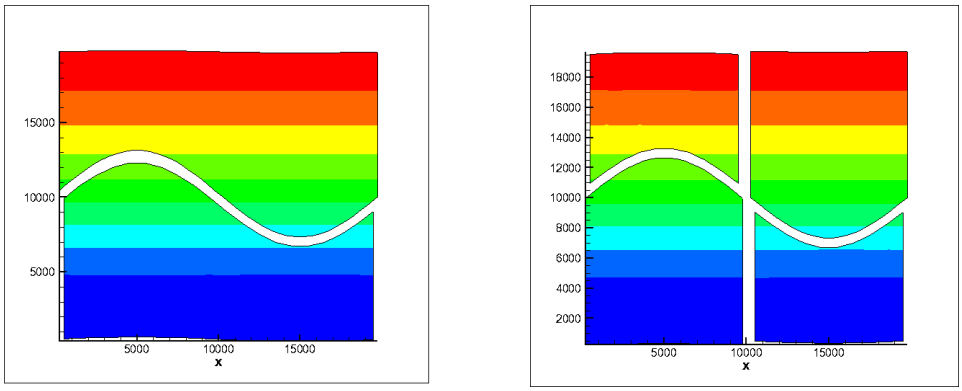



Figure 7: Isolines of $(T_r)_K$ in cell centers on Non-matching sine meshes. $(a)$ Two subdomains. $(b)$ Four subdomains.

**Remark 6.1.** There are many factors working on the convergence rate of Lions domain decomposition algorithm. The Robin parameter is one of factors, and some references [9, 15] focus on the optimal Robin parameter and optimized Schwarz methods for the linear equation. We believe that the nonlinear term is another one and it may be affect the optimal Robin parameter. Here, we are interested in the accuracy of our algorithm on non-matching meshes for radiation diffusion equations.

**Acknowledgments** This work was supported by the National Natural Science Foundation of China (11471047, 91118001, 11271053, 91330107), Science Foundation of China Academy of Engineering Physics (2013B0202034) and Defense Industrial Technology Development Program (B1520133015).

## References

[1] I. AAVATSMARK, T. BARKVE, O. BOE, T. MANNSETH, *Discretization on non-orthogonal, quadrilateral grids for inhomogeneous, anisotropic media*, J. Comput. Phys., vol.127,

https://doi.org/10.4208/nmtma.2015.m1403 Published online by Cambridge University Press

(1996), pp. 2-14.
[2] I. Aavatsmark, E. Reiso, R. Teigland, *Control-volume discretization method for quadrilateral grids with faults and local refinements*, Comput. Geosci., (2001), pp. 1-23.
[3] Y. Achdou, C. Japhet, Y. Maday, F. Nataf, *A new cement to glue nonconforming grids with Robin interface conditions: the finite volume case*, Numer. Math., vol.92, no.4, (2002), pp. 593-620.
[4] M. Berndt, K. Lipnikov, M. Shashkov, M. F. Wheeler, I. Yotov, *Superconvergence of the velocity in mimetic finite difference methods on quadrilaterals*, SIAM J. Numer. Anal., vol.43, (2005), pp. 1728-1749.
[5] F. Brezzi, K. Lipnikov, V. Simoncini, *A family of mimetic finite difference methods on polygonal and polyhedral meshes*, Math. Mod. Methods. Appl. Sci. vol.15, (2005), pp. 1533-1551.
[6] Q. Y. Chen, J. Wan, Y. Yang, R. T. Mifflin, *Enriched multi-point flux approximation for general grids*, J. Comput. Phys., vol.227, (2008), pp. 1701-1721.
[7] R. E. Ewing, R. D. Lazarov, P. S. Vassilevski, *Local refinement techniques for elliptic problems on cell-centered grids*, i: Error analysis. Math. Comput., vol.56, no.194, (1991), pp. 437-461.
[8] S. Fu, H. Fu, L. Shen, S. Huang, G. Chen, *A nine point difference scheme and iteration solving method for two dimensional energy equations with three temperatures*, Chinese J. Comput. Phys., vol.15, no.4, (1998), pp. 489-497.
[9] M. J. Gander, *Optimized Schwarz methods*, SIAM J. Numer. Anal. vol.44, no.2, (2006), pp. 699-731.
[10] T. Gu, Z. Dai, X. Liu, *Partial Newton-Krylov iterative methods for a system of energy equations with three-temperatures*, Numerical Heat Transfer, Part B, vol.53, (2008), pp. 1-12.
[11] J. Hyman, J. Morel, M. Shashkov, S. Steinberg, *Mimetic finite difference methods for diffusion equations*, Comput. Geosci., vol.6 (2002), pp. 333-352.
[12] R. A. Klausen, R. Winther, *Robust convergence of multi point flux approximation on rough grids*, Numer. Math., vol.104, (2006), pp. 317-337.
[13] D. A. Knoll, W. J. Rider, G. L. Olson, *An efficient nonlinear solution method for nonequilibrium radiation diffusion*, J. Quant. Spectrosc. Radiat. Transfer, vol.63, (1999), pp. 15-29.
[14] K. Lipnikov, M. Shashkov, I. Yotov, *Local flux mimetic finite difference methods*, Numer. Math., vol.112, (2009), pp. 115-152.
[15] S. H. Lui, *A Lions non-overlapping domain decomposition method for domains with an arbitrary interface*, IMA J. Numer. Anal., vol.29, no.2, (2009), pp. 332-349.
[16] J. E. Morel, R. M. Roberts, M. J. Shashkov, *A local support-operators diffusion discretization scheme for quadrilateral r-z meshes*, J. Comput. Phys., vol.144, (1998), pp. 17-51.
[17] V. A. Mousseau, D. A. Knoll, *Temporal accuracy of the nonequilibrium radiation diffusion equations applied to two-dimensional multimaterial simulations*, Nuclear Sci. Engrg., vol.154, (2006), pp. 174-189.
[18] V. A. Mousseau, D. A. Knoll, W. J. Rider, *Physics-based preconditioning and the Newton-Krylov method for non-equilibrium radiation diffusion*, J. Comput. Phys., vol.160, (2000), pp. 743-765.
[19] C. C. Ober, J. N. Shadid, *Studies on the accuracy of time-integration methods for the radiation-diffusion equations*, J. Comput. Phys., vol.195, (2004), pp. 743-772.
[20] G. L. Olson, L. H. Auer, M. L. Hall, *Diffusion, P1, and other approximate forms of*

https://doi.org/10.4208/nmtma.2015.m1403 Published online by Cambridge University Press

*radiation transport*, J. Quantum Spectrosc. Radiat. Transger, vol.64, (2000), pp. 619-634.
[21] Y. SAAD, *Iterative method for sparse linear systems*, New York :PWS publishing, 1996.
[22] L. SAAS, I. FAILLE, F. NATAF, F. WILLIEN, *Finite volume methods for domain decomposition on nonmatching grids with arbitrary interface conditions*, SIAM J. Numer. Anal., vol.43, (2005), pp. 860-890.
[23] Z. SHENG, G. YUAN, *A nine point scheme for the approximation of diffusion operators on distorted quadrilateral meshes*, SIAM J. Sci. Comput., vol.30, (2008), pp. 1341-1361.
[24] Z. SHENG, J. YUE, G. YUAN, *Monotone finite volume schemes for nonequilibrium radiation diffusion equations on distorted meshes*, SIAM J. Sci. Comput., vol.31, (2009), pp. 2915-2934.
[25] J. WU, Z. DAI, Z. GAO, G. YUAN, *Linearity preserving nine-point schemes for diffusion equation on distorted quadrilateral meshes*, J. Comput. Phys., vol.229, (2010), pp. 3382-3401.
[26] L. YIN, J. WU, Z. GAO, *The cell functional minimization scheme for diffusion problems on unstructured polygonal meshes*, ESAIM: M2AN,vol.49,(2015), pp.193-220.
[27] L. YIN, J. WU, Y. YAO, *A cell functional minimization scheme for parabolic problem*, J. Comput. Phys., vol.229, (2010), pp. 8935-8951.
[28] L. YIN, J. WU, Y. YAO, *A cell functional minimization scheme for domain decomposition method on non-orthogonal and non-matching meshes*, Numer. Math., vol.128, (2014), pp.773-804.
[29] G. YUAN, Z. SHENG, *Monotone finite volume schemes for diffusion equations on polygonal meshes*, J. Comput. Phys., vol.227, (2008), pp. 6288-6312.
[30] Y. ZHANG ET. AL., *Computational investigation of the magneto-Rayleigh-Taylor instability in Z-pinch implosions*, Phys. Plasmas., vol.17, no.4, (2010), 042702.

https://doi.org/10.4208/nmtma.2015.m1403 Published online by Cambridge University Press